Validation of Snow Cover Fraction for Regional Climate Simulations in the Sierra Nevada

Melissa L. Wrzesien[1], Tamlin M. Pavelsky[2], Sarah B. Kapnick[3], Michael T. Durand[4], Thomas H. Painter[5]

[1]School of Earth Sciences, The Ohio State University, Columbus, OH, USA
[2]Department of Geological Sciences, University of North Carolina at Chapel Hill, Chapel Hill, NC, USA
[3]Program in Atmospheric and Oceanic Sciences, Princeton University, and NOAA/Geophysical Fluid Dynamics Laboratory, Princeton, NJ, USA
[4]School of Earth Sciences and Byrd Polar Research Center, The Ohio State University, Columbus, OH, USA
[5]Jet Propulsion Laboratory, California Institute of Technology, Pasadena, CA, USA

0. Abstract

Mountain snow cover plays an important role in regional climate due to its high albedo, its effects on atmospheric convection, and its influence on lower-elevation runoff. Snowpack water storage is also a critical water resource and understanding how it varies is of great social value. Unfortunately, *in situ* measurements of snow cover are not widespread; therefore, models are often depended on to assess snowpack and snow cover variability. Here, we use a new satellite-derived snow product to evaluate the ability of the Weather Research and Forecasting (WRF) regional climate model with the Noah land surface model with multiparameterization options (Noah-MP) to simulate snow cover fraction (SCF) and snow water equivalent (SWE) on a 3 km domain over the central Sierra Nevada. WRF/Noah-MP SWE simulations improve upon previous versions of the Noah land surface model by removing the early bias in snow melt. As a result, WRF/Noah-MP now accurately simulates spatial variations in SWE. Additionally, WRF/Noah-MP correctly identifies the areas where snow is present and captures large-scale variability in SCF. Temporal RMSE of the domain-average SCF was 1863.9 km^2 (24%). However, our study reveals that WRF/Noah-MP struggles to simulate SCF at the scale of individual grid cells. The equation used to calculate SCF fails to produce temporal variations in grid-scale SCF and depletion occurs too rapidly. Therefore SCF is a nearly binary metric in

mountain environments. Sensitivity tests of the equation may improve simulation of SCF during accumulation or melt but does not remove the bias for the entire snow season. Though WRF/Noah-MP accurately simulates the presence or absence of snow, high-resolution, reliable SCF measurements may only be attainable if snow depletion equations are designed specifically for complex topographical areas.

1. Introduction

The presence or absence of snow is an important component of climate in mountainous regions. Snow has a high albedo compared to most other land cover types, so its presence substantially decreases the amount of solar radiation absorbed by the land surface and inhibits radiative warming of the atmosphere. As snow melts, the underlying land surface is revealed, the amount of absorbed solar radiation increases, and atmospheric temperature increases. This process governs the snow-albedo feedback that acts to cool the surface when there is expansive snow cover (Groisman *et al.*, 1994; Namias, 1985). The positive snow-albedo feedback amplifies warming in snow-covered mountain environments on seasonal to multidecadal timescales (Déry and Brown, 2007). Snow cover fraction (SCF), the fractional portion of the surface covered by snow, also impacts the convective activity of the atmosphere through the changes in latent and sensible heat associated with melt and snowfall (Zhang, 2005). From an ecological perspective, the presence of snow prevents soil and roots from freezing (Groffman *et al.*, 2001) and helps to maintain adequate soil moisture levels (Yeh *et al.*, 1983). Finally, mountainous regions and areas downstream of montane headwaters rely heavily on snowmelt runoff for water supplies throughout the year. Snowpack acts as a natural reservoir by storing winter precipitation and releasing water during spring snowmelt (Barnett *et al.*, 2005). At present, runoff from melt generally coincides with higher demand during the summer. However, should snow begin to

melt earlier in the season due to warmer temperatures that result from anthropogenic climate forcing, there may be water shortages, especially in regions that do not have adequate capacity to store early snow melt. With an estimated one-sixth of the global population living in regions that depend on snowpack, water resources could be strained for millions of people (Barnett *et al.*, 2005). The Sierra Nevada in California is one such area since it provides 60% of Southern California's water supply through snowpack (Waliser *et al.*, 2009), yet the reservoirs must be managed to balance the needs of water storage and flood prevention. Reduced snow cover could alter the region's radiative balance and exacerbate the problem of already scarce water resources. Recent studies suggest that the melt season and the onset of spring are already occurring earlier in the western United States (Cayan *et al.*, 2001; Hamlet *et al.*, 2005; Mote *et al.*, 2005; Kapnick and Hall, 2012). However few SCF validation studies have been done, and it is uncertain whether regional climate models can accurately reproduce observed spatial and temporal patterns in SCF.

In this study, we aim to validate a model simulation of SCF over the central Sierra Nevada. The majority of past modeling studies of mountain snowpack have focused on snow water equivalent (SWE), not SCF, because SWE is important for water resources (Rasmussen *et al.*, 2011) and SCF is difficult to measure in the field. Though *in situ* SCF data are hard to obtain, measurements can instead be taken from space with satellite-based sensors. Remote sensing methods map snow cover either through a binary flag ("snow" or "no snow") or as SCF (Nolin, 2010). Although space-based measurements of snow cover are becoming more widely used, they are complicated by clouds and vegetation. Crane and Anderson (1984) used near-infrared (NIR) reflectance to differentiate clouds and snow, which have similar reflectances in visible wavelengths. In NIR wavelengths, snow is not highly reflective and appears dark while clouds

appear bright. Vegetation poses difficulties because forests inhibit visibility of snow beneath the canopy and add to the pixel's reflectance signature (Nolin, 2010). Here we use a SCF product derived from NASA's Moderate Resolution Imaging Spectroradiometer (MODIS), the MODIS Snow-Covered Area and Grain size (MODSCAG) algorithm (Painter *et al.*, 2009), with a correction to estimate SCF under vegetation. MODSCAG calculates the SCF of each MODIS pixel using spectral reflectances of snow based on snow grain size and other land-cover types. MODSCAG is a physical-based algorithm optimized for mountainous environments, and has shown good accuracy in past studies. Rittger *et al.* (2013) found MODSCAG SCF RMSE of 0.10 in mountainous terrain. Thus in this study, we validate WRF SCF by comparison against MODSCAG.

This study extends previous work by Pavelsky *et al.* (2011), here after referred to as PKH2011, which validated the accumulation and melt of snowpack in the central Sierra Nevada via WRF V3.1/Noah. Here, we validate SCF in two different versions of WRF/Noah (V3.1 and the more recent V3.4 with a new land surface model, Noah-MP) against MODIS-derived measurements of daily SCF (Painter *et al.*, 2009) for the same time period and spatial extent used by PKH2011. The latest version of WRF/Noah has incorporated significant improvements to the SWE scheme but has yet to be validated in the Sierra Nevada and for maritime snow. Validation of the WRF/Noah-MP SCF against a high-quality, near-daily SCF product will provide the first analysis of how well regional climate models simulate SCF in mountain environments.

2. Models and Data

Model Setup

The National Center for Atmospheric Research and several collaborating institutions developed the WRF model for operational weather forecasting and regional climate and meteorological studies (Skamarock *et al.*, 2008). In this study, we use both WRF V3.1 (with the Noah land surface model (LSM)) and WRF V3.4 (with the newer Noah-MP LSM) to investigate the evolution of SCF and SWE over the period November 2001 through September 2002 for the central Sierra Nevada (Figure 1a). Version 3.1 uses the Noah LSM, which has multiple soil layers but only a single layer of snowpack that is combined with surface soil and the vegetation canopy (Chen and Dudhia, 2001; Ek *et al.*, 2003). In WRF V3.4, there is an option to use Noah-MP, a new Noah LSM with multiparameterization options (Niu *et al.*, 2011). We use Noah-MP because prior studies suggest improved simulation of SWE (Niu *et al.*, 2011). In Noah-MP, snow is modeled separately from soil using up to three distinct snow layers, depending on snow depth. Noah-MP also has a new method of calculating SCF based on snow density, SWE, and snow depth as compared to Noah, in which SCF is based on SWE and snow depth alone (Ek *et al.*, 2003; Koren *et al.*, 1999). During the ablation season, the SCF equation describes the snow depletion curve (SDC) of how the SCF changes as the snowpack melts. A model run using WRF V3.4 with Noah has similar results to WRF V3.1/Noah, leading us to believe the version of WRF does not significantly contribute to changes in SCF or SWE simulation.

All simulations are run with three nested domains at increasingly fine resolution – 27, 9, and 3 km – though here we focus on the 3 km domain because prior work suggests that this resolution is necessary to capture orographic processes to first order (Pavelsky *et al.*, 2011). The lateral boundary conditions for the 27 km domain and the initial conditions (at time step 0) come from the North American Regional Reanalysis (NARR) product (Mesinger *et al.*, 2006), while each higher resolution domain receives boundary conditions from the domain enclosing it.

Simulation results are output on a 3-hour timestep. As such, simulations of all three domains are run concurrently, with larger domains processed before smaller domains at each individual timestep.

We selected the following WRF physics options: the Thompson *et al.* (2008) cloud microphysics scheme, the rapid radiative transfer model longwave scheme (Mlawer *et al.*, 1997), the Dudhia shortwave scheme (Dudhia, 1989), the Yonsei University planetary boundary layer scheme (Hong *et al.*, 2006), and the modified Kain-Fritsch convective parameterization for the two outer domains (Kain, 2004; Kain and Fritsch, 1990, 1993).

Remotely Sensed Data

Using NASA's Moderate Resolution Imaging Spectroradiometer (MODIS), a sensor on-board the Terra and Aqua satellites, Painter *et al.* (2003) developed the MODIS Snow-Covered Area and Grain size (MODSCAG) algorithm, which calculates SCF in 500x500 m grid cells. Here we use the latest version of MODSCAG, version 3, with SCF corrections for vegetated areas (Painter *et al.*, personal communication). Though we focus primarily on version 3, we will show one comparison with MODSCAG version 2, which did not have the vegetation correction (Painter *et al.*, 2009). In version 2, accurate detection of SCF was limited in forest environments because MODSCAG cannot calculate SCF beneath canopies. In version 3, those limitations are addressed. We chose to use MODSCAG for validation because it is physical-based and optimized for mountain environments. The MODSCAG algorithm is a multiple endmember method that uses linear spectral analysis to solve for SCF and grain size for each pixel. An endmember is the spectral reflectance of a pure surface cover, such as snow. The scheme developed by Painter *et al.* (2009) uses multiple endmembers for snow based on different snow grain sizes. The linear spectral analysis assumes that measured radiance is a linear combination

of the reflectances of the surface features. MODSCAG uses the MODIS MOD09GA product, which is an atmospherically corrected surface hemispherical-directional reflectance factor, to avoid misclassification of clouds as snow and vice versa.

In order to develop a daily SCF product, we first replace cloudy pixels in each image with SCF measurements from the most recent previous clear-sky image. On average, we replaced ~26% of each scene (2400x2400 pixels) to remove cloudy areas. For days where there was no data due to a satellite processing problem or some other error (a total of 13 days), we simply used the previous day's measurements.

Study Area and In Situ Measurements

The innermost model domain covers an area of 34,992 km^2 that includes the Central Sierra Nevada Mountains and parts of California's Central Valley. Four watersheds are fully located within the study area: the Stanislaus, the Tuolumne, the Merced, and the San Joaquin. WRF simulated elevations range from 61 m to 3646 m with an average elevation of 1561 m. Elevations above 1500 m have an average annual maximum vegetation fraction of 48% with a dominant vegetation type of evergreen needleleaf, according to the WRF land use classification.

To evaluate WRF SWE values, we used snow pillow data measured by pressure-sensing pillows. Inside the 3x3 km domain, there are 41 snow pillow sites (shown as black dots in Figure 1b) with daily observations acquired from the California Department of Water Resources Data Exchange Center (http://cdec.water.ca.gov). Nine stations operated by the Natural Resources Conservation Service are part of the SNOTEL network. All stations are at elevations above 1875 m with an average elevation of 2607 m. The average maximum SWE measured by the snow pillows for our study period is 65.9 cm. The same 41 locations were used in PKH2011.

3. Methods of Assessing Model Performance

Snow Water Equivalent Timing

In order to examine how Noah and Noah-MP differ in simulation of snowpack in the central Sierra Nevada, we compare the timing of snowmelt following the methods of PKH2011. We use SWE centroid date (SCD) to assess model skill in simulating snowpack timing. SCD is the date the center of snowpack mass occurs (Kapnick and Hall, 2010). The SCD is computed as:

$$SCD = \frac{\sum t_i SWE_i}{\sum SWE_i}$$

Where t_i is the number of days since November 1 and SWE_i is each day's SWE measurement in millimeters. PKH2011 indicated that, on average, simulated SCD occurred 22 - 25 days early in WRF V3.1/Noah compared to snow pillow observations. We replicate the method presented by PKH2011 of regressing the difference between modeled and observed SCD against the difference in elevation between each observation point and the corresponding model grid cell (Figure 2), which allows us to assess the ability of WRF V3.4/Noah-MP to produce unbiased estimates of snowpack accumulation and ablation timing. Model grid cells and point-based observations will always have inherent differences due to area-averaging in models (most notably with elevation), so individual modeled SCD values are unlikely to match observed values. However, we assume that the error in snowpack timing due to scale differences is randomly distributed once corrected for elevation bias. As such, if the physics within the model are correct, the y-intercept of the regression line between SCD and elevation differences should be close to zero.

Snow Cover Fraction

We use three different methods to validate WRF/Noah simulations of SCF:

First, we compare geographic extent of snow cover by mapping the output of WRF and MODSCAG together. The spatial plots provide a visual comparison of the two datasets throughout the entire season. Prior to any quantitative analysis, this provides an opportunity to see the time periods when WRF and MODSCAG have large discrepancies. For example, versions of WRF/Noah up through v3.1 have consistently struggled to simulate snowpack during the melt season (Figure 3d, Livneh *et al.*, 2010).

Second, we compare the total snow covered area (SCA) in WRF and MODSCAG over the entire innermost WRF domain. We use two methods to study SCA. First, we count the number of snowy pixels. Since MODSCAG is not able to detect SCF below 0.15 (Painter *et al.*, 2009), we consider a pixel to be snowy if it has at least a SCF value of 0.15. The snowy pixel metric gives an indication if WRF/Noah-MP is simulating approximately the correct number of grid cells with snow present. However, this does not consider the individual SCF values. Second, total SCA is calculated by multiplying the SCF value for each grid cell by the dataset's resolution (9 km^2 for WRF and 0.25 km^2 for MODSCAG). Here we additionally compare MODSCAG V2 SCA to the vegetation-corrected MODSCAG V3 SCA to assess the importance of the vegetation correction.

Finally, we compare the mean SCF in unvegetated pixels in WRF and MODSCAG. We choose to only consider sparsely vegetated areas due to the effects of vegetation on SCF. To determine whether accuracy of land cover classification impacts our results, we use two different products: the native WRF land cover map and the MODIS land cover classification (Friedl *et al.*, 2002). WRF characterizes land cover based on the United States Geological Survey's (USGS) 24 land use categories (Wang, 2012). We also use the MODIS land cover classification scheme. Since there are 36 MODIS pixels in one WRF pixel, we consider a WRF cell to be

9

sparsely vegetated under the MODIS scheme if it contains at least 20 unvegetated MODIS pixels (55%) within the WRF grid cell. Figure 3 shows the differences in pixel selection from the two methods with 53 unvegetated pixels in the WRF scheme and only 41 MODIS-aggregated pixels. WRF unvegetated pixels are more distributed across various elevation classes with more found at low elevations. We do not consider unvegetated grid cells below 2200 m because they do not represent the mountainous environments with which we are primarily concerned. We match each of the remaining 44 unvegetated WRF pixel to the mean of the 36 corresponding MODSCAG pixels and compare daily SCF.

4. Results

Snow Water Equivalent

Comparison of SCD error and elevation difference between snow pillows and WRF pixels in WRF V3.1/Noah and WRF V3.4/Noah-MP (Figure 2) reveals a substantial improvement in simulation of snowpack accumulation and especially in melt timing. Linear regression analysis determines y=0.039x+2.08 to be the line of best fit with a R^2 value of 0.536. This result suggest that WRF V3.4/Noah-MP simulates the SCD ~2 days late when there is no elevation biased present, compared to 22 days early in WRF V3.1/Noah. With a p-value of 0.0775, the 2 day bias of WRF V3.4/Noah-MP SCD is significant only at the 90% confidence level.

Snow Cover Fraction

Visual comparison of snow cover extent in WRF V3.4/Noah-MP and MODSCAG reveals both similarities and occasional differences between WRF and MODSCAG. Overall, visual comparison suggests that the boundaries of SCA are well matched in WRF V3.4/Noah-MP and MODSCAG. However there are exceptions, especially in the early season when SCA is

rapidly increasing (Figure 4a-c). These differences are likely due to cloud contamination of MODSCAG. Should a snowstorm move into the area, WRF captures the increase in snow cover as it occurs (Figure 4a), but MODSCAG must wait for clear skies to confirm a change in snow cover (Figure 4b). A reliable model simulation of SCF would provide a continuous SCF record regardless of clouds.

While there are sometimes discrepancies in SCA early in the accumulation season, WRF V3.4/Noah-MP and MODSCAG are generally in agreement during mid-winter when snow cover is at its greatest extent. On January 1 (Figure 4d-f), which represents a typical mid-winter day, the geographic boundaries of snow cover in the two datasets match closely. In Figure 4e, MODSCAG SCF values near 1.0 (red areas) cover a large portion of the region, which match high SCF values in WRF V3.4/Noah-MP (Figure 4d). However, WRF V3.4/Noah-MP still tends to have less variability. The snow cover extent of the two datasets on April 1 (Figure 4g-i) matches reasonably well. During the melt season, the eastern boundary of WRF V3.4/Noah-MP and MODSCAG are in agreement, but WRF V3.4/Noah-MP has more snowy pixels toward the western edge of the Sierra Nevada (Figure 4j-l).

We investigate the snow cover to reveal any apparent biases in snowpack extent over the whole domain. First we evaluate the number of snowy pixels (i.e. where SCF > 0.15, Figure 5). The seasonal cycle in the number of snowy pixels allows us to determine the accuracy of WRF/Noah simulations. As with SWE metrics, there is an improvement in WRF V3.4/Noah-MP over V3.1/Noah during the melt season. While WRF V3.1/Noah simulates melt early, producing a snow-free domain a month before MODSCAG, WRF V3.4/Noah-MP shows more gradual melt, closely matching observed patterns from MODSCAG. Especially during summer melt in June and July WRF V3.4/Noah-MP and MODSCAG are in near-perfect agreement, in

comparison to the large discrepancies between WRF V3.1/Noah and MODSCAG during these months. For the rest of the year, neither WRF V3.4/Noah-MP nor MODSCAG show a bias relative to the other. The two datasets have similar variability and WRF even reproduces the transient peaks of SCA associated with storm events seen in MODSCAG. The root mean squared error (RMSE) between WRF V3.4/Noah-MP and MODSCAG is 206.5 (21%) snowy pixels. The overestimation of snowy pixels from April to July in the WRF V3.4/Noah-MP simulation likely contributes to the majority of the RMSE.

We also analyze total SCA by comparing the simulated WRF V3.4/Noah-MP value with both versions of MODSCAG, the original and the vegetation-corrected version (Figure 6). By correcting for the presence of vegetation, the SCA as observed by MODSCAG dramatically increases. While both datasets have similar SCA magnitudes during melt in June and July, other months show increases of almost 10,000 km^2 in the vegetation-corrected MODSCAG. Considering the amount of snow under canopies has a large effect on the total SCA. The corrected MODSCAG closely matches the WRF V3.4/Noah-MP total SCA from November through April. Only once melt begins do the two datasets begin to differ. The RMSE between the simulated and observed total SCA is 1863.9 km^2 (24%) for MODSCAG V3 and 4588.8 km^2 (100%) for MODSCAG V3. After adjusting for vegetation, MODSCAG and WRF V3.4/Noah-MP are in better agreement for total SCA.

Though the WRF V3.4/Noah-MP results indicate improvements in SCA simulation over the whole domain, examination of SCF in a single land-cover type may reveal potential biases. In the WRF and the MODIS land cover products, sparsely vegetated areas make up only about 1% of the WRF domain, largely at the highest elevations in the southern portion of the study area (Figure 3). Both land cover classification schemes show similar, but not identical, unvegetated

regions. In each case, WRF SCF values in unvegetated regions are higher than MODSCAG values throughout the period of snow cover (Figure 7). WRF also shows less variability during the peak snowpack season between December and April. The fact that WRF SCF stays near 1.0 suggests that once WRF determines a 3x3 km cell is snow-covered, it remains so for the rest of the season. MODSCAG, which demonstrates more variability, exhibits more gradual increases and decreases in SCF than either version of WRF. For WRF V3.4/Noah-MP, unvegetated SCF increases to 0.8 in 3 days, compared to 31 days in MODSCAG. During ablation in the summer, SCF decreases from a snow accumulation event in late May to an average SCF value of less than 0.01 over 44 days for WRF V3.4/Noah-MP and 55 days for MODSCAG. WRF V3.1/Noah and WRF V3.4/Noah-MP show similar patterns (a plateau effect) through May when the records begin to deviate. While both LSMs show a quick decease in SCF, Noah declines a month earlier than Noah-MP. By early June, Noah no longer classifies any of the unvegetated pixels as having a substantial SCF. In contrast, Noah-MP has snow cover to the beginning of July. During the spring melt, when Noah SCF values for unvegetated pixels approximate zero, Noah-MP has values ~0.8.

The high values of SCF for unvegetated areas in WRF suggest that WRF treats SCF as a binary metric in mountainous regions where snowpack is deep. SCF for the barren regions of the Sierra Nevada essentially plateaus near 1.0 from December to May/June. To determine whether this is true only for high-elevation unvegetated pixels or whether it is common to all WRF pixels, we compare the mean monthly SCF for all WRF pixels in the domain to the average of the 36 corresponding MODSCAG pixels. A two-pixel buffer zone around the edge of the model domain is removed due to model artifacts in these areas. The whole-domain output for WRF V3.4/Noah-MP (Figure 8) shows that the Noah-MP LSM nearly always classifies pixels as either no snow or

fully covered. Particularly in March and April, SCF in WRF V3.4/Noah-MP is essentially

binary, with either snow (SCF = 1) or no snow (SCF = 0). Very few values fall in between. In

contrast, MODSCAG exhibits a wide range of values of SCF.

5. Discussion and Conclusion

Our results indicate that WRF with the Noah-MP LSM can, on average, accurately

simulate SWE for mountainous environments. One of the largest problems with WRF V3.1/Noah

found in PKH2011, early snowmelt, has been addressed in WRF V3.4/Noah-MP. We see an

improvement in the simulated timing of SCD in WRF V3.4/Noah-MP compared with WRF

V3.1/Noah. Therefore WRF V3.4/Noah-MP can likely be used to simulate temporal variability

in snowpack in poorly observed mountain environments, which includes most of the world's

mountainous regions outside the Western United States. Additionally, the ability to reliably

model SWE suggests that we can simulate future changes in snowpack associated with

anthropogenic climate forcings. Reliable model projections can prepare communities for future

conditions, including changes in water supply quantity and timing.

For the whole-domain SCF, WRF V3.4/Noah-MP improves upon WRF V3.1/Noah and

has realistic variability that matches the observations from MODSCAG. Figure 6 in particular,

showing total SCA, suggests that WRF V3.4/Noah-MP closely matches the new vegetation-

corrected MODSCAG, with similar SCA magnitudes for the entire winter until melt begins.

However, averaging over the entire domain also hides potential biases in some land cover types.

In particular, there are biases in how WRF V3.4/Noah-MP handles unvegetated areas. The binary

pattern of SCF in WRF is a product of the snow depletion equation included in Noah-MP. Niu

and Yang (2007) implemented the following equation for SCF into Noah-MP:

$$f_{sno} = \tanh\left(\frac{h_{sno}}{2.5z_{0g}\left(\frac{\rho_{sno}}{\rho_{new}}\right)^m}\right)$$

Where h_{sno} is snow depth in meters, z_{0g} is the ground roughness length (equal to 0.01 m), ρ_{sno} is snow density in kg m^{-3}, ρ_{new} is fresh snow density (equal to 100 kg m^{-3}), and m is a dimensionless melting factor. The default m value is 1.0.

When using typical values of snow depth and snow density for the central Sierra Nevada, we can calculate the expected value of SCF (Figure 9a, based on Figure 1b from Niu and Yang (2007)). Regardless of snow density, at a depth of 0.2 m Noah-MP calculates a SCF value of at least 0.9. This compares to typical snow depth values in the central Sierra Nevada in WRF V3.4/Noah-MP of 0.5 – 1.5 m during the snow-covered season. As a result, a melting factor of 1.0 leads to SCF curves that quickly become fully snow covered.

With larger values of m, the SCF requires deeper snow to reach full cover (Figure 9b). Therefore greater m values may lead to a better match between WRF and MODSCAG. We re-ran WRF V3.4/Noah-MP with m values of 1.6 (suggested in Niu and Yang (2007) for coarse resolution models), 2.5, and 5.0. Scatterplots for SCF values comparing WRF and MODSCAG are shown in Figure 10. Large values of m (m = 5.0, as in Figure 10g-i) have points clustered on the one-to-one line when snow is accumulating (November and December) but does not simulate conditions well in January. In contrast, smaller values of m (m = 1.6, 2.5 in Figures 10a-c, 10d-f, respectively) may work better in January. A single equation for the entire year limits how well the model can simulate the range of possible conditions.

Besides altering the Noah-MP equations, improvements in SCF simulation could come from new methods of modeling SCF. A snow-depletion curve that is optimized for mountain environments could potentially improve simulation of SCF in WRF. Considering the fact that

Noah-MP struggles with modeling SCF in individual mountainous pixels (Niu and Yang, 2007), a new parameterization based on actual snow cover depletion in mountain environments could solve the problem of near-binary snow cover WRF V3.4/Noah-MP. Several studies have developed SDCs to improve simulation of snowpack ablation. SDCs have been modeled as a three parameter lognormal distribution (Donald *et al.*, 1995), a two parameter lognormal distribution (Liston, 2004), and as a two parameter Gamma distribution (Kolberg and Gottschalk, 2006). Often a SDC is coupled with models to improve energy balance and mass balance calculations (Donald *et al.*, 1995; Luce and Tarboton, 2004). Most of the depletion equations require knowledge of the coefficient of variation of the snow cover for the region of interest (Donald *et al.*, 1995; Liston, 2004; Luck and Tarboten, 2004; Girotto *et al.*, 2013). Girotto *et al.* (2013) demonstrate that the SDC developed by Liston (2004) can be coupled to a LSM to reconstruct montane snowpack in the Sierra Nevada without *in situ* data, providing the potential for wide spread use on regions without numerous observations. Future work could incorporate the Liston (2004) SDC into WRF/Noah-MP to attempt to improve SCA simulation during the ablation season.

For the whole domain of the central Sierra Nevada, regional models can simulate SCA with reasonable accuracy. WRF V3.4/Noah-MP captures the seasonal pattern of SCA when compared with MODSCAG SCA values. WRF V3.4 and Noah-MP, in combination, produce simulations that would be useful for future predictions of SCA for the entire region. However on a pixel-by-pixel basis, WRF V3.4/Noah-MP fails to accurately simulate SCF and produces artificially binary SCF values. Biases in unvegetated regions indicate that models cannot yet simulate SCF over a grid cell with a heterogeneous surface. The ability to perform these simulations accurately has important ramifications for simulation of the surface energy balance

16

and related atmospheric conditions. Without mountain-specific SCF formulations, discrepancies between model and observational SCF values are likely to persist.

6. Acknowledgements

7. References

Barnett TP, Adam JC, Lettenmaier DP. 2005. Potential impacts of a warming climate on water availability in snow-dominated region. *Nature* **438:** 303-309. DOI: 10.1038/nature04141.

Cayan DR, Kammerdiener SA, Dettinger MD, Caprio JM, Peterson DH. 2001. Changes in the onset of spring in the Western United States. *Bulletin of the American Meteorological Society* **82:** 399-415. DOI: 10.1175/1520-0477(2001)082<0399:CITOOS>2.3.CO;2.

Chen F, Dudhia J. 2001. Coupling an advanced land-surface/hydrology model with the Penn State/NCAR MM5 modeling system. Part I: Model description and implementation. *Monthly Weather Review* **129:** 569-585. DOI: 10.1175/1520-0493(2001)129<0569:CAALSH>2.0.CO;2.

Crane RG, Anderson MR. 1984. Satellite discrimination of snow/cloud surfaces. *International Journal of Remote Sensing* **5:1:** 213-223. DOI: 10.1080/01431168408948799.

Déry SJ, Brown RD. 2007. Recent Northern Hemisphere snow cover extent trends and implications for the snow-albedo feedback. *Geophysical Research Letters* **34:** L22504. DOI: 101.1029/2007GL031474.

Donald JR, Soulis ED, Kouwen, N, Pietroniro A. 1995. A Land Cover-Based Snow Cover Representation for Distributed Hydrologic Models. *Water Resources Research* **31:** 995-1009. DOI: 10.1029/94WR02973.

Dudhia J. 1989. Numerical study of convection observed during the winter monsoon experiment using a mesoscale two-dimensional model. *Journal of the Atmospheric Sciences* **46:** 3077-3107. DOI: 10.1175/1520-0469(1989)046<3077:NSOCOD>2.0.CO;2.

Ek MB, Mitchell KE, Lin Y, Rogers E, Grunmann P, Koren V, Gayno G, Tarpley JD. 2003. Implementation of Noah land surface model advances in the National Centers for Environmental Prediction operational mesoscale Eta model. *Journal of Geophysical Research* **108:** D228851. DOI: 10.1029/2002JD003296.

Friedl MA, McIver DK, Hodges JCF, Zhang XY, Muchoney D, Strahler AH, Woodcock CE, Gopal S, Schneider A, Cooper A, Baccini A, Gao F, Schaaf C. 2002. Global land cover mapping from MODIS: algorithms and early results. *Remote Sensing of Environment* **83:** 287-302. DOI: 10.1016/S0034-4257(02)00078-0.

Girotto M, Margulis SA, Durand M. 2013. Probabilistic SWE reanalysis as a generalization of deterministic SWE reconstruction techniques. *Hydrological Processes*. DOI: 10.1002/hyp.9887.

Groffman PM, Driscoll CT, Fahey TJ, Hardy JP, Fitzhugh RD, Tierney GL. 2001. Colder soils in a warmer world: A snow manipulation study in a northern hardwood forest ecosystem. *Biogeochemistry* **56:** 135-150. DOI: 10.1023/A:1013039830323.

Groisman PY, Karl TR, Knight RW. 1994. Observe impact of snow cover on the heat balance and the rise of continental spring temperatures. *Science* **263:** 198-200. DOI: 10.1126/science.263.5144.198.

Hamlet AF, Mote PW, Clark MP, Lettenmaier DP. 2005. Effects of Temperature and Precipitation Variability on Snowpack Trends in the Western United States. *Journal of Climate* **18:** 4545-4561. DOI: 10.1175/JCLI3538.1.

Hong SY, Noh Y, Dudhia J. 2006. A new vertical diffusion package with an explicit treatment of entrainment processes. *Monthly Weather Review* **134:** 2318-2341. DOI: 10.1175/MWR3199.1.

Kain J. 2004. The Kain-Fritsch convective parameterization: An update. *Journal of Applied Meteorology* **43:** 170-181. DOI: 10.1175/1520-0450(2004)043<0170:TKCPAU>2.0.CO;2.

Kain JS, Fritsch JM. 1990. A one-dimensional entraining/detraining plume model and its application in convective parameterization. *Journal of the Atmospheric Sciences* **47:** 2784-2802. DOI: 10.1175/1520-0469(1999)047<2784:AODEPM>2.0.CO;2.

Kain JS, Fritsch JM. 1993. Convective parameterization for mesoscale models: The Kain-Fritsch scheme, in The Representation of Cumulus Convection in Numerical Models. *Meteorological Monographs*, vol. 46, edited by K. A. Emanuel and D. J. Raymond, pp. 165–170, American Meteorological Society: Reston, Va.

Kapnick S, Hall A. 2010. Observed climate-snowpack relationships in California and their implications for the future. *Journal of Climate* **23:** 3446-3456. DOI: 10.1175/2010JCLI2903.1.

Kapnick S, Hall A. 2012. Causes of recent changes in western North American snowpack. *Climate Dynamics* **38:** 1885-1899. DOI: 10.1007/s00382-011-1089-y.

Kolberg SA, Gottschalk L. 2006. Updating of snow depletion curve with remote sensing data. *Hydrological Processes* **20:** 2363-2380. DOI: 10.1002/hyp.6060.

Koren V, Schaake J, Mitchell K, Duan QY, Chen F, Baker JM. 1999. A parameterization of snowpack and frozen ground intended for NCEP weather and climate models. *Journal of Geophysical Research* **104:** 19569-19585. DOI: 10.1029/1999JD900232.

Liston GE. 2004. Representing Subgrid Snow Cover Heterogeneities in Regional and Global Models. *Journal of Climate* **17:** 1381-1397. DOI: 10.1175/1520-0442(2004)017<1381:RSSCHI>2.0.CO;2.

Livneh B, Xia Y, Mitchell KE, Ek MB, Lettenmeier DP. 2010. Noah LSM Snow Model Diagnostics and Enhancements. *Journal of Hydrometeorology* **11:** 721-738. DOI: 10.1175/2009JHM1174.1.

Luce CH, Tarboten DG. 2004. The application of depletion curves for parameterization of subgrid variability of snow. *Hydrological Processes* **18:** 1409-1422. DOI: 10.1002/hyp.1420.

Mlawer EJ, Taubman SJ, Brown PD, Iacono MJ, Clough SA. 1997. Radiative transfer for inhomogeneous atmospheres: RRTM, a validated correlated-k model for the long wave. *Journal of Geophysical Research* **102:** 16663-16682. DOI: 10.1029/97JD00237.

Mote PW, Hamlet AF, Clark MP, Lettenmaier DP. 2005. Declining mountain snowpack in western North America. *Bulletin American Meteorological Society* **86:** 39-49. DOI: 10.1175/BAMS-86-1-39.

Namias J. 1985. Some empirical evidence for the influence of snow cover on temperature and precipitation. *Monthly Weather Review* **113:** 1542-1553. DOI: 10.1175/1520-0493(1985)113<1542:SEEFTI>2.0.CO;2.

Niu GY, Yang ZL. 2007. An observation-based formlation of snow cover fraction and its evaluation over large North American river basins. *Journal of Geophysical Research* **112:** D21101. DOI: 10.1029/2007JD008674.

Niu GY, Yang ZL, Mitchell KE, Chen F, Ek MB, Barlage M, Kumar A, Manning K, Niyogi D, Rosero E, Tewari M, Xia Y. 2011. The community Noah land surface model with multiparameterization options (Noah-MP): 1. Model description and evaluation with local-scale measurements. *Journal of Geophysical Research* **116:** D12109. DOI: 10.1029/2010JD015139.

Nolin AW. 2010. Recent advances in remote sensing of seasonal snow. *Journal of Glaciology* **56:** 1141-1150. DOI: 10.3189/002214311796406077.

Painter TH, Dozier J, Roberts DA, Davis RE, Green RO. 2003. Retrieval of subpixel snow-covered area and grain size from imaging spectrometer data. *Remote Sensing of Environment* **85:** 64–77. DOI: 10.1016/S0034-4257(02)00187-6.

Painter TH, Rittger K, McKenzie C, Slaughter P, Davis RE, Dozier J. 2009. Retrieval of subpixel snow covered area, grain size, and albedo from MODIS. *Remote Sensing of Environment* **113:** 868-879. DOI: 10.1016/j.rse.2009.01.001.

Pavelsky TM, Kapnick S, Hall A. 2011. Accumulation and melt dynamics of snowpack from a multiresolution regional climate model in the central Sierra Nevada, California. *Journal of Geophysical Research* **116:** D16115. DOI: 10.1029/2010JD015479.

Skamarock WC, Klemp JB, Dudhia J, Gill DO, Barker DM, Duda M, Huang X, Wang W, Powers JG. 2008. A description of the advanced research WRF version 3. *Techical Note 475*, National Center for Atmospheric Research, Boulder, Colorado.

Thompson G, Field P, Rassmussen RM, Hall W. 2008. Explicit forecasts of winter precipitation using an improved bulk microphysics scheme. Part II: Implementation of a new snow parameterization. *Monthly Weather Review* **136:** 5095-5115. DOI: 10.1175/2008MWR2387.1.

Waliser D, Kim J, Xue Y, Chao Y, Eldering A, Fovell R, Hall A, Li Q, Liou KN, McWilliams J, Kapnick S, Vasic R, De Sale F, Yu Y. 2009. Simulating the cold season snowpack: The impact of snow albedo and multi-layer snow physics. California Climate Change Center.

Wang W, Bruyere C, Duda M, Dudhia J, Gill D, Kavulich M, Keene K, Lin HC, Michalakes J, Rizvi S, Zhang X. 2012. Advanced Research WRF (ARW) Version 3.4 Modeling Users Guide. Mesoscale & Microscale Meteorology Division, National Center for Atmospheric Research, Boulder, USA.

Wang Z, Zeng X, Decker M. 2010. Improving snow processes in the Noah land model. *Journal of Geophysical Research* **115:** D20108. DOI: 10.1029/2009JD013761.

Yeh TC, Wetherald RT, Manabe S. 1983. A model study of the short-term climatic and hydrologic effects of sudden snow cover removal. *Monthly Weather Review* **111:** 1013-1024. DOI: 10.1175/1520-0493(1983)111<1013.AMSOTS>2.0.CO;2.

Zhang T. 2005. Influence of the seasonal snow cover on the ground thermal regime: An overview. *Review of Geophysics* **43:** RG4002. DOI: 10.1029/2004RG000157.

8. Figures
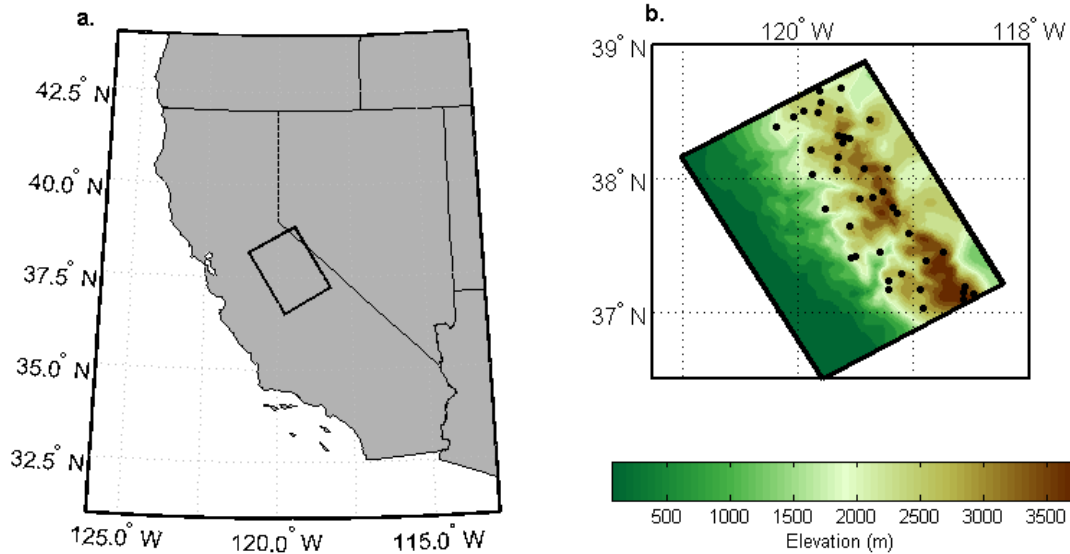
Figure 1. (a) Model domain of the central Sierra Nevada for the 3 km WRF simulation. (b) Simulated topography from WRF V3.4/Noah-MP. Elevation is in meters. Black dots indicate locations of snow pillows.
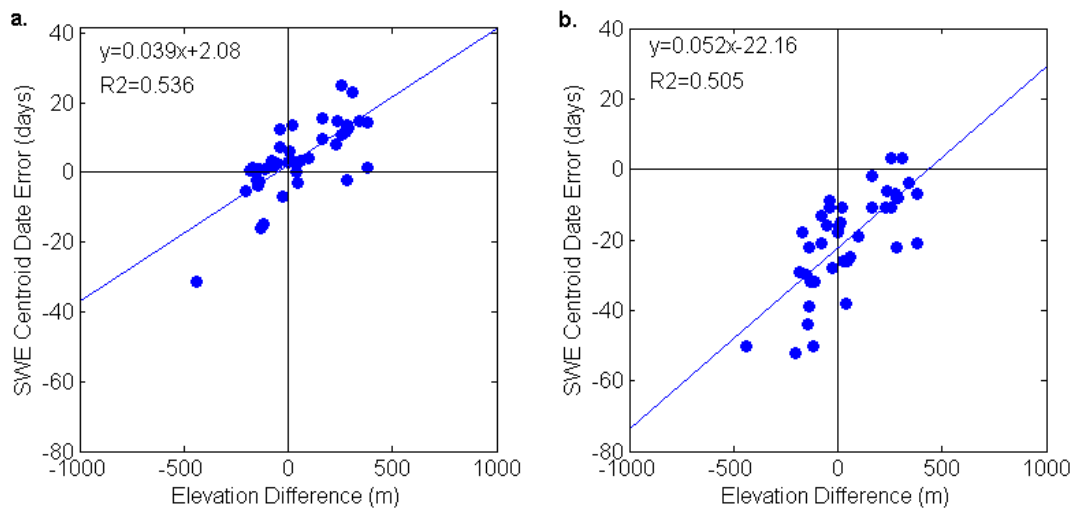
Figure 2. SWE centroid date (SCD) error and elevation difference between model simulations and snow pillow observations. (a) WRF V3.4/Noah-MP shows substantial improvement in SCD simulation compared to (b) WRF V3.1/Noah. Subplot (b) is reproduced from Figure 7c in PKH2011.
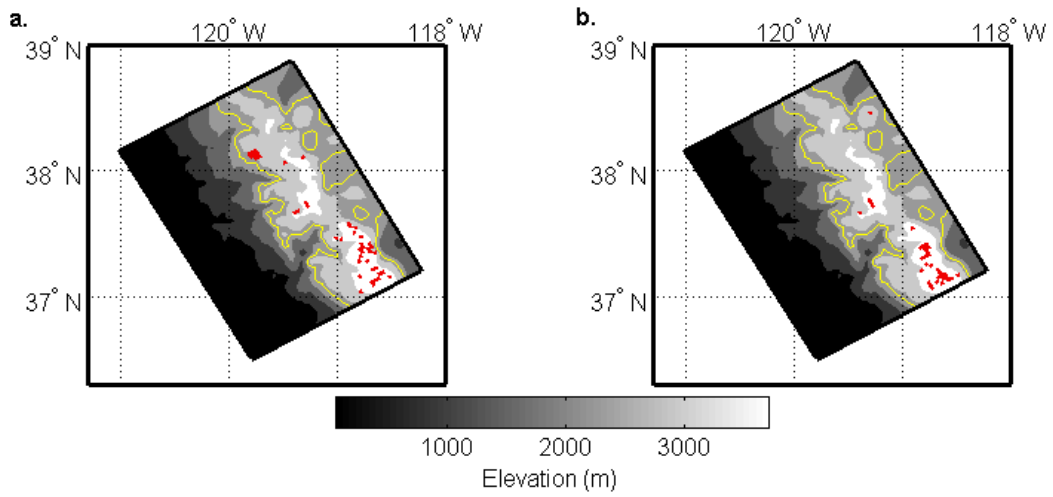
Figure 3. Unvegetated pixels in the land cover classification scheme in (a) WRF and (b) MODIS. The yellow line separates elevations above and below 2200 m.
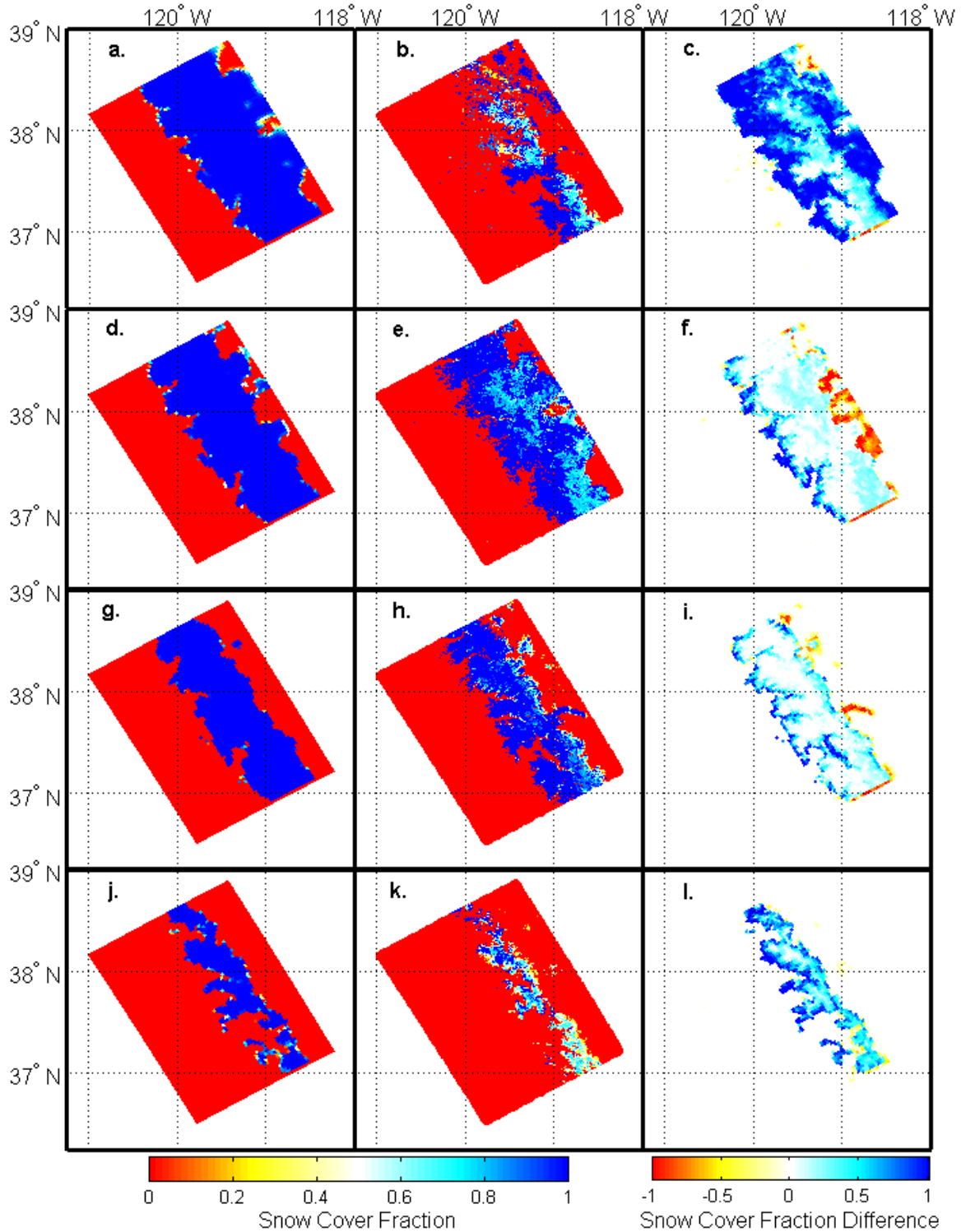
Figure 4. Snow cover extent comparison WRF V3.4/Noah-MP and MODSCAG over the model domain on (a-c) November 25, (d-f) January 1, (g-i) April 1, and (j-l) June 1. The left column is WRF V3.4/Noah-MP SCF, the center column is MODSCAG SCF, and the right column is the difference in SCF values between WRF V3.4/Noah-MP and MODSCAG.
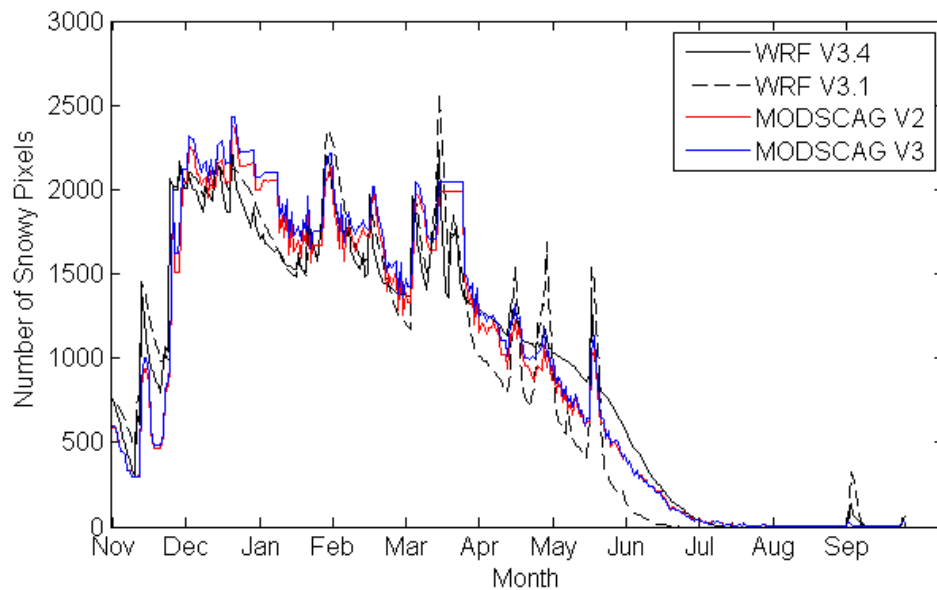
Figure 5. Comparison of the number of domain-wide "snowy" pixels for WRF V3.4, WRF V3.1, and MODSCAG V3. A pixel is classified as snowy for SCF > 0.15. Results for MODSCAG V2 are not shown as they are almost identical to V3.
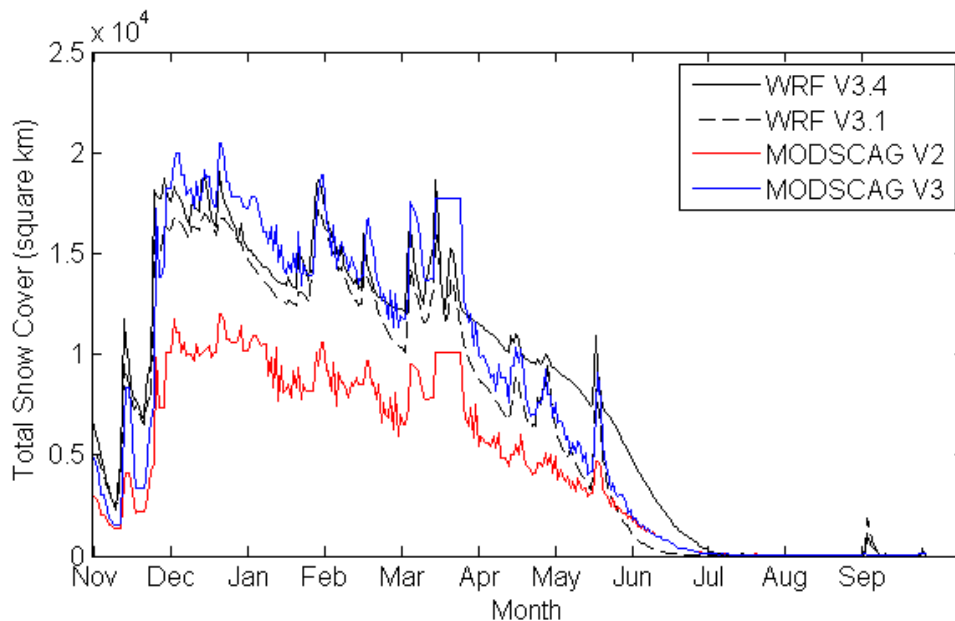
Figure 6. Total snow cover (in km^2) of the model domain. The black line is WRF V3.4/Noah-MP, the dotted black line is WRF V3.1/Noah, the red line is MODSCAG V2, and the blue line is the vegetation-corrected MODSCAG V3. Correcting for snow cover under canopies results in WRF and MODSCAG being in close agreement for a large portion of the study period.
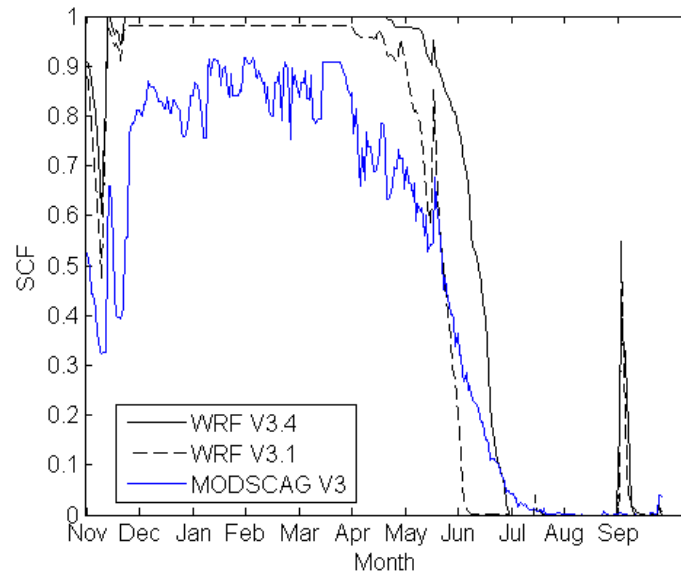
Figure 7. Seasonal pattern of average SCF values for unvegetated pixels above 2200 m for the WRF land cover classification scheme. A similar pattern was found for the MODIS land cover classificaiton scheme, though not shown here.
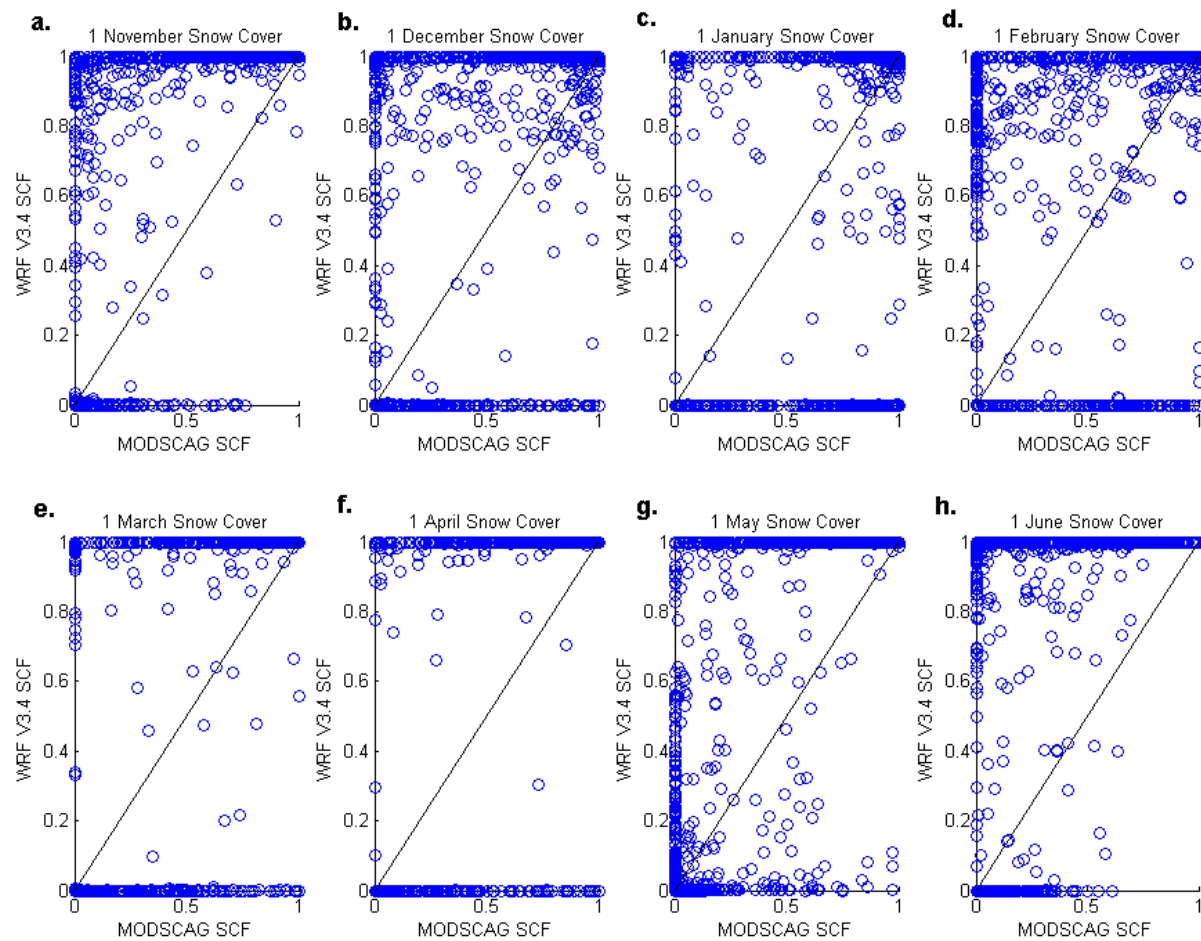
Figure 8. Scatterplots for WRF V3.4/Noah-MP SCF values vs. MODSCAG SCF values over the entire domain. In each plot, WRF V3.4/Noah-MP becomes a binary SCF classifier.
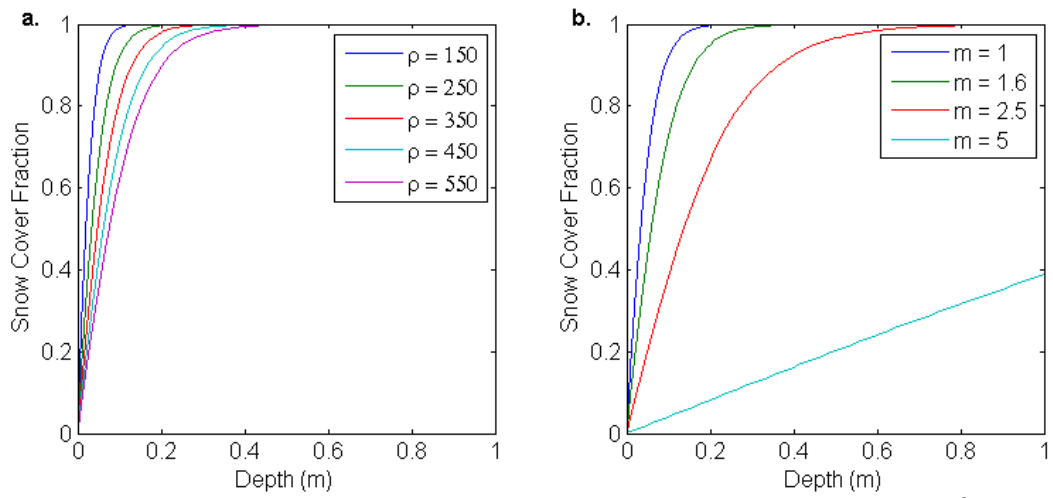
Figure 9. Expected SCF value based on snow depth (m) and snow density (kg m^{-3}). Reproduced from Figure 1b from Niu and Yang (2007).
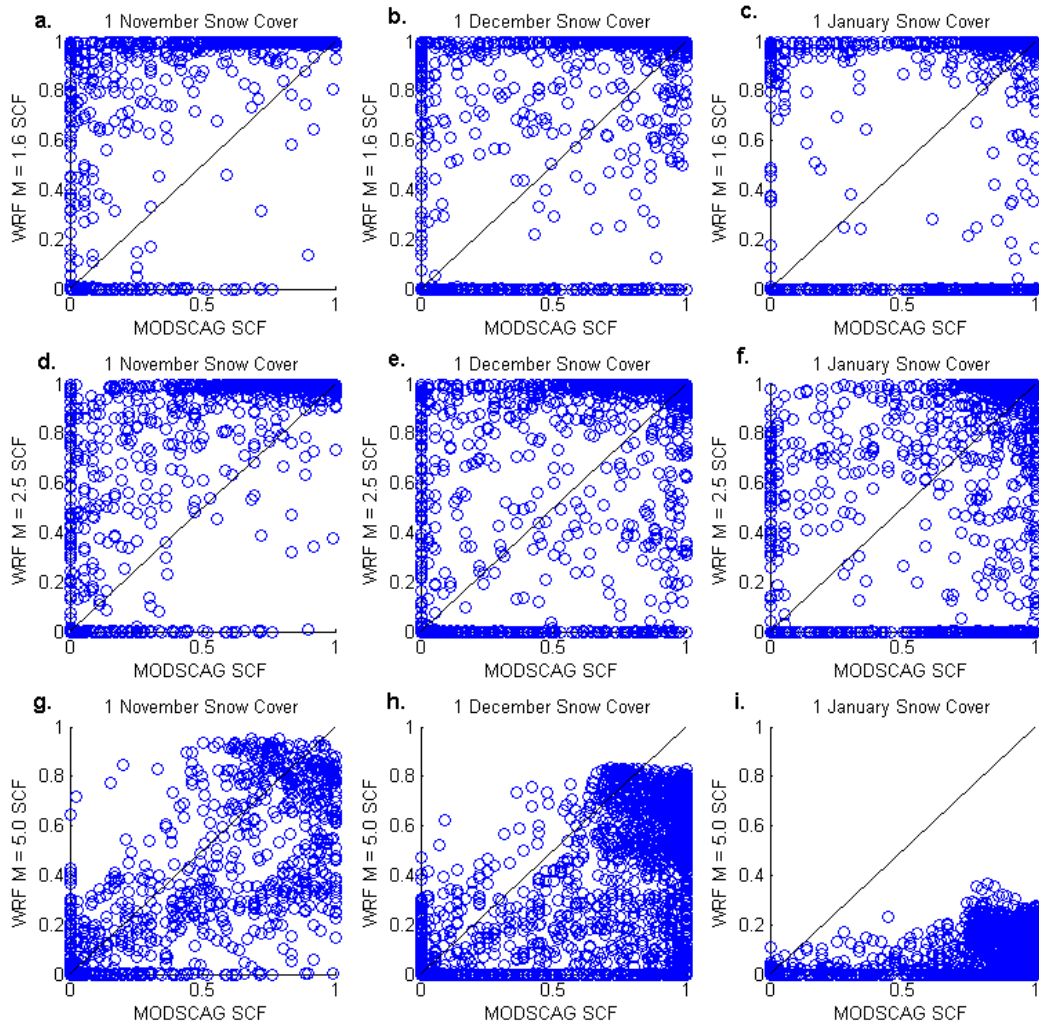
Figure 10. Scatterplots of WRF SCF vs. MODSCAG SCF for different melting factors, m, over the entire model domain. The top row is m=1.6, the middle is m=2.5, and the bottom row is m=5.0. At higher m values, WRF V3.4/Noah-MP stops behaving as a binary flag and shows increased variability in SCF values.